esting composite laminates for energy absorbing ability can be accomplished well with the 64-mm-wide specimen. It is stable, not affected by the edge constraints, and yields a comparable SSCS value to that of the tube specimens. The ease with which the 64-mm-wide specimen can undergo off-axis testing is also beneficial for investigating the energy absorption characteristics of composites. Moreover, the flat-plate is more economical for energy absorption laminate screening because of the ease of manufacture and testing.

ACKNOWLEDGMENTS

This work was supported by the Army Research Office under contract No. DAAH-0493-G0001. Dr. Thomas Doligalski was the contract monitor. The authors wish to thank Mr. William R. Pogue, III and Dr. David C. Fleming for their help in this effort.

REFERENCES

1. J. K. Sen and C. C. Dremann, "Design Development Tests for Composite Crashworthy Helicopter Fuselage," *SAMPE Quarterly*, Vol. 17, No. 1, Oct. 1985, pp. 29–39.
2. D. C. Fleming and A. J. Vizzini, "Tapered Geometries for Improved Crashworthiness under Side Loads," *Journal of the American Helicopter Society*, Vol. 17, No. 1, Jan. 1993, pp. 38–44.
3. G. L. Farley, "Energy Absorption of Composite Materials," *Journal of Composite Materials*, Vol. 17, No. 5, May 1983, pp. 267–279.
4. D. Hull, "A Unified Approach to Progressive Crushing of Fibre-Reinforced Composite Tubes," *Composites Science and Technology*, Vol. 40, pp. 377–421, 1991.
5. Jackson, K., J. Morton, J. A. Lavoie, R. Boitnott. "Scaling of Energy Absorbing Composite Plates," *Journal of the American Helicopter Society*, Vol. 39, No. 1, Jan. 1994, pp. 17–23.
6. J. A. Lavoie and J. Morton, "A Crush Test Fixture for Investigating Energy Absorption of Flat Composite Plates," *Experimental Techniques*, Nov/Dec 1994, pp. 23–26.
7. D. C. Fleming and A. J. Vizzini, "The Energy Absorption of Composite Plates under Off-Axis Loads," *Journal of Composite Materials*, Vol. 30, No. 18, 1996, pp. 1977–1995.
8. G. L. Farley, "Energy Absorption of Composite Material and Structure," *Proceedings of the AHS 43rd Annual Forum*, St. Louis, MO, May 1987, pp. 613–627.

Design Optimization of Fiber Reinforced Plastic Composite Shapes

PIZHONG QIAO,* JULIO F. DAVALOS*,† AND EVER J. BARBERO**
West Virginia University
Morgantown, WV 26506-6103

(Received September 27, 1996)
(Revised June 27, 1997)

ABSTRACT: A global approximation method to optimize material architecture and cross-sectional area of new fiber reinforced plastic (FRP) composite beams is presented. The sections considered are intended for applications in short-span bridges. The beams are subjected to transverse loading, and the optimization constraints include deflection limit, material failure, and elastic buckling. Assuming a laminated structure for the pultruded FRP shapes, experimentally-verified micro/macromechanics models are used to predict member structural behavior. The design variables include the cross-sectional geometric dimensions and the material architecture. The constraint functions are defined through a global approximation at a number of design points, and the approximate constraint equations are obtained through multiple linear regressions and are defined as power law functions of the design variables. The proposed method can concurrently optimize the dimensions and material architecture of a given shape, and as an illustration, a new winged-box (WB) shape is optimized. The present optimization approach combined with existing knowledge on FRP shapes can be used to develop various new shapes and to create a new family of efficient FRP geometries for the civil structural market.

KEY WORDS: deflection, elastic buckling, failure, global approximation, power law, material architecture, pultrusion, FRP shapes, optimization, laminated beam.

1. INTRODUCTION

FIBER-REINFORCED PLASTIC (FRP) beams and columns are increasingly used in civil engineering structures, because of their favorable properties, such as light weight, electromagnetic transparency, noncorrosive, and high energy absorption. FRP structural shapes are being considered either to replace or complement the traditional steel, aluminum, wood, and concrete structural members. FRP shapes are typically manufactured using glass fibers and either polyester or vinyl

*Department of Civil and Environmental Engineering.
**Department of Mechanical and Aerospace Engineering.
†Author to whom correspondence should be addressed.

0021-9983/98/02 0177–20 $10.00/0

ester resins. The shapes are commonly produced by pultrusion, a continuous process capable of delivering one to five feet per minute of prismatic thin/thick-walled members, or by a recently developed vacuum assisted resin transfer molding process—Seeman Composite Resin Infusion Molding Process (SCRIMP). With significant recent improvements made in pultrusion manufacturing and the potential shown by the SCRIMP process, the production of large FRP structural shapes for construction of bridges and buildings is a reality.

Current FRP structural shapes used in civil engineering are similar to existing steel shapes, which were designed by trial-and-error and by market acceptance of the best shapes over a long period of time. However, this process may or may not apply to FRP shapes. The significant progress made in the quality of constituents, fiber and resin systems, has been incorporated into FRP shapes over the years, but the majority of the geometric shapes simply emulate existing steel shapes. Thus, the concern is that the current and not optimum FRP shapes may not be accepted by the construction market, because of the relatively low performance-to-cost ratio of current sections, and therefore, FRP shapes may not have the chance to evolve in the marketplace in a similar way as steel shapes have.

A particularly attractive advantage of FRP composites is the ability to tailor the material system along with the geometric shape for a given application. The full potential applications of composites could be realized by concurrently designing the material system and structural shape to attain a desirable structural behavior. This advantageous characteristic of pultruded FRP composites can be exploited to overcome controlling constraints, such as deflection limit, material failure, and critical buckling load. The purpose of this paper is to combine existing knowledge on analysis and design of FRP shapes with innovative optimization techniques to formulate an optimization procedure for new FRP composite structural shapes. The important considerations in design and analysis of optimal FRP shapes for structural applications are discussed, and the present technique can be used to develop various new shapes. We envision that by developing optimally designed sections, the evolution and acceptance time for FRP shapes in the civil infrastructure market can be accelerated.

Unlike the extensive work reported for laminated composite plates and shells [1,2], the material architecture and shape optimization of thin-walled and moderately-thick-walled laminated composite beams is still under investigation and is less developed. Burnside et al. [3] proposed a design optimization of an all-FRP bridge deck; cellular box and stiffened box geometries were optimized with considerations of deflection and buckling in their studies. Morton and Webber [4] developed a procedure for obtaining an optimal (minimum area) design of a composite I-beam with regard to structural failure, local buckling, and midspan deflection; by using an iterative design-and-test strategy combined with heuristic redesign rules and a complex method, they obtained an optimal solution in terms of a set of cross-sectional dimensions. Davalos, Qiao, and Barbero [5] recently proposed a multiobjective (multicriteria) design optimization of material architecture (ply fiber orientations and ply fiber percentages) for pultruded FRP shapes. A wide flange I-section beam, which is one of the most commonly used structural shapes, was chosen to illustrate the analysis and design optimization; the beam maximum

deflection, buckling resistance, and material failure were considered as multiple objectives (criteria) in the optimization process. The optimal solutions were obtained through a multiobjective scheme, and a recommended practical material architecture design was proposed, which was used to manufacture and test actual sections.

In this paper, we present a global approximation method to concurrently optimize the material architecture and cross-sectional area of a new pultruded FRP shape. The member is subjected to transverse bending loading, and the optimization constraints include deflection limit, material failure, and elastic buckling, all of which depend on the material system (lay-up) and the cross-sectional geometry (shape) of the member. The design variables include the cross-sectional geometric dimensions and material architecture. The constraint functions are defined through a global approximation at a number of design points, and the approximate constraint equations are obtained using multiple linear regressions to generate power law functions of the design variables. We use statistical tools to assess goodness-of-fit of the constraint approximations. The overall optimization scheme is used in conjunction with the commercial program IDESIGN [6] to obtain the optimal solution for the design problem.

2. CHARACTERIZATION OF PLY MATERIAL AND LAMINATE PROPERTIES

The modeling of FRP shapes requires several material properties, primarily longitudinal and transverse moduli and strengths and in-plane shear stiffness and strength for each layer of each panel of the cross section. These properties need to be predicted during the optimization process as functions of the design variables. Most pultruded FRP sections, such as wide-flange, box, and other shapes, consist typically of arrangements of flat walls or panels. Usually, the reinforcement used is E-glass fiber, and the resin or matrix is either vinyl ester or polyester. Although pultruded FRP shapes are not laminated structures in a rigorous sense, they are pultruded with material architectures that can be simulated as laminated configurations [7]. A typical pultruded section may include the following four types of layers [8]: (1) A thin layer of randomly-oriented chopped fibers (Nexus) placed on the surface of the composite. This is a resin-rich layer primarily used as a protective coating, and its contribution to the laminate response can be neglected; (2) Continuous Strand Mats (CSM) of different weights, consisting of continuous randomly-oriented fibers; (3) Stitched Fabrics (SF) with different angle orientations, which commonly used 0°/90° and ±45° orientations in practical designs [5]; and (4) Roving layers that contain continuous unidirectional fiber bundles, which contribute the most to the stiffness and strength of a section.

This study is concerned with the design optimization of material architecture and dimensions of FRP shapes, consisting of E-glass fibers and vinyl ester matrix. The material properties of the constituents (E-glass fiber and vinyl ester matrix) are considered to be isotropic [8]. The material architecture of the component panels includes sets of continuous strand mats (CSM), ±45° stitched fabrics (SF), and rovings (unidirectional fibers) arranged through the thickness of each panel. A

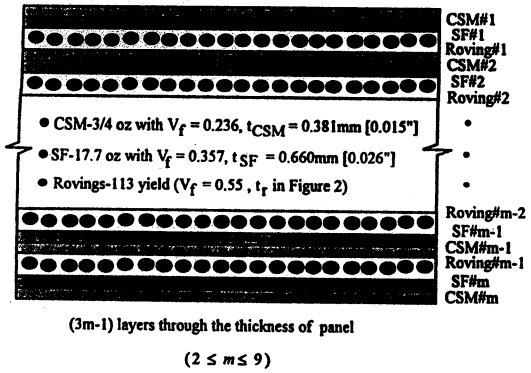

Figure 1. *Simulation of idealized panel lay-up system for pultruded FRP shapes.*

ymmetric lay-up is considered consisting of an idealized $(3m - 1)$ number of lay-rs with m CSM layers, m SF layers, and $(m - 1)$ roving layers, as shown in Figure . The idealized layer thicknesses of CSM, SF and roving layers (t_{CSM}, t_{SF} and t_r) nd their corresponding fiber volume fractions [$(V_f)_{CSM}$, $(V_f)_{SF}$ and $(V_f)_r$] are evalu-ted using the information provided by the material producer and pultrusion anufacturer (see Reference [8]), and each layer is modeled as a homogeneous, nearly elastic, and generally orthotropic material. The ply materials used are ecified as 0.229 kg/m^2 [3/4 oz/ft^2] CSM, 0.6 kg/m^2 [17.7 oz/yd^2] SF, and 227.6 /kg [113 yield (yard/lb)] roving, which are commercially available and com-only used in pultruded FRPs. The units used in this study are oz for CSM and SF nd yield for rovings, because these units are widely accepted in manufacturing nd design. The ply thicknesses (t_{CSM} and t_{SF}) are given in Figure 1, and the fiber olume fractions for CSM [$(V_f)_{CSM}$] and SF [$(V_f)_{SF}$] layers are obtained following avaols et al. [8]. The fiber volume fraction of a roving layer is assumed as $(V_f)_r$ = 5% in this study. The total thickness of a panel, t, is defined as

$$t = mt_{SF} + mt_{CSM} + (m - 1)t_r \tag{1}$$

here, for a given roving layer thickness (t_r) and lay-up number (m), the panel ickness, t, can be computed from Equation (1).

For a roving layer, the number of rovings per unit width (mm^{-1} or [in^{-1}]), N_r, can e independently computed by knowing t_r and $(V_f)_r$ as

$$N_r = Y\rho_r(V_f)_r t_r \tag{2}$$

here the yield (Y = 227.6 m/kg [113 yard/lb] in this study) and density (ρ_r = 0546 kg/m^3 [0.092 lb/in^3] for E-glass fiber) are given by the material producer ee Reference [8]). The fiber percentages of SF, CSM, and roving layers in a nel can be defined as

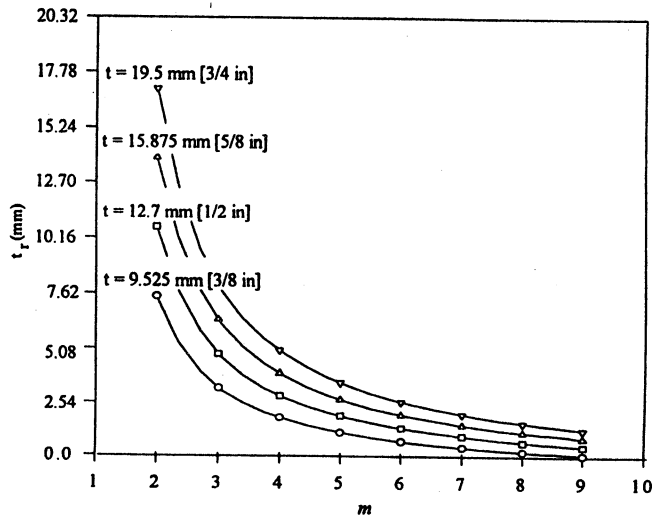

Figure 2. *Panel thickness (t) as function of lay-up number (m) and roving layer thickness (t_r).*

$$X_{CSM} = \frac{m(V_f)_{CSM}t_{CSM}}{t} \times 100\%, \quad X_{SF} = \frac{m(V_f)_{SF}t_{SF}}{t} \times 100\%$$
$$X_r = \frac{(m-1)(V_f)_r t_r}{t} \times 100\% \tag{3}$$

In this study, the design variables for material architecture are the lay-up number (m) and roving layer thickness (t_r). By knowing m and t_r for a panel of an FRP shape, the panel thickness (t), number of rovings (N_r), and the fiber percentages of SF, CSM, and roving layers can be obtained. The relationship between the variables m and t_r with respect to the panel thicknesses is plotted in Figure 2. Considering current manufacturing practices, the following upper and lower bounds are imposed on the design variables of material architecture:

$$2 \le m \le 9$$
$$0.0508\,\text{mm}\,[0.002]\,\text{in} \le t_r \le 17.018\,\text{mm}\,[0.67\,\text{in}] \tag{4}$$

For pultruded sections, it is not practical to evaluate the ply stiffnesses through experimental tests, since the material is not produced by lamination lay-up. The ply stiffnesses can be computed from several formulas of micromechanics of composites [8]. In this study, we compute the ply stiffnesses (Table 1) using a micromechanics model for composites with periodic microstructure [9]. Ply strength values cannot be predicted by standard micromechanics models developed for aerospace-type composites. A new set of micromechanics models, sometimes in-

Table 1. Engineering constants of typical layers in pultruded laminates.

Layer	V_f	E_1 (GPa)	E_2 (GPa)	G_{12} (GPa)	ν_{12}	$X^*_{T/C}$ (MPa)	$Y^*_{T/C}$ (MPa)	S^* (MPa)
3/4 oz. CSM	0.236	11.989	11.989	4.290	0.398	145.854	58.150	28.958
17.7 oz. ±45° SF	0.357	28.481	8.744	3.136	0.339	661.297	58.150	28.958
Rovings (113 yield)	0.550	41.825	12.239	4.820	0.282	661.297	58.150	28.958

*$X_{T/C}$, $Y_{T/C}$ = longitudinal and transverse strengths in tension/compression; S = shear strength.

cluding empirical correction factors, have been developed and correlated with experimental data by Makkapati [10], Sonti [11], and Tomblin [12]. In this study, we predict first-ply-failure (FPF) based on the ply strengths evaluated from existing models [10–12].

3. ANALYSIS OF FRP SHAPES

Because of the complexity of composite materials, analytical and design tools developed for members of conventional materials can not always be readily applied to FRP shapes, and numerical methods, such as finite elements, are often difficult and expensive to use and require specialized training. Therefore, a comprehensive engineering approach for analysis and design of pultruded FRP shapes has been developed. The analyses of FRP beams for elastic, failure, and buckling responses are briefly discussed next.

3.1 Deflection Predictions

In this study, the response of FRP shapes in bending is evaluated using the Mechanics of thin-walled Laminated Beams (MLB) model [13]; a formal engineering approach based on kinematic assumptions consistent with Timoshenko beam theory. MLB can be applied to FRP structural shapes with either open or closed cross-sections consisting of assemblies of flat walls; it is suitable for straight FRP beam-columns with at least one axis of geometric symmetry. For each laminated wall (e.g., a flange or a web), the compliance matrices $[\alpha]_{3\times3}$, $[\beta]_{3\times3}$, and $[\delta]_{3\times3}$ are obtained from classical lamination theory (CLT) [14]. Incorporating stress resultant assumptions compatible with beam theory without torsion and assuming that the off-axis plies are balanced symmetric ($\alpha_{16} = \beta_{16} = 0$; for most pultruded FRP sections, the off-axis plies are manufactured with balanced symmetric patterns), the extensional, bending-extension coupling, bending, and shear stiffnesses of each panel are expressed as:

$$\overline{A}_i = (\delta_{11}\Delta^{-1})_i, \quad \overline{B}_i = (-\beta_{11}\Delta^{-1})_i, \quad \overline{D}_i = (\alpha_{11}\Delta^{-1})_i$$
$$\overline{F}_i = (\alpha_{66}^{-1})_i \quad \text{where } \Delta = \alpha_{11}\delta_{11} - \beta_{11}^2 \tag{5}$$

For each panel, a contour coordinate of the middle surface is defined in terms of the vertical coordinate as (Figure 3)

$$y(s_i) = s_i \sin\phi_i + \bar{y}_i \quad \text{for } -\frac{b_i}{2} \le s_i \le \frac{b_i}{2} \tag{6}$$

where b_i is the panel width, $\bar{y}_i$ is the location of the panel centroid with respect to a global coordinate x–y, and ϕ_i is the orientation of the ith panel.

General expressions for the beam stiffness coefficients are derived from the beam variational problem. Hence, axial (A_z), bending-extension coupling (B_x or

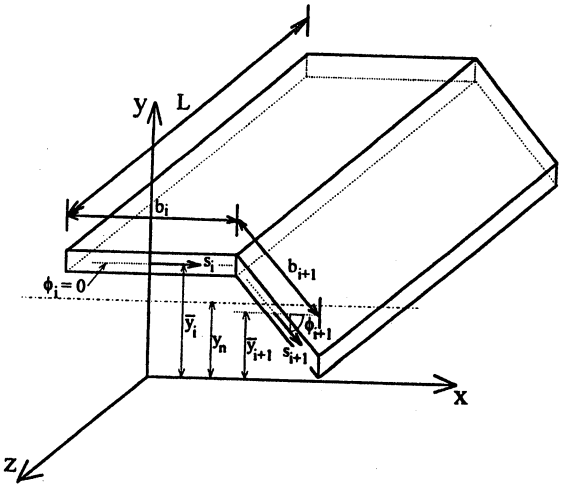

Figure 3. *Thin-walled panel geometry and contour coordinate.*

B_y), bending (D_x or D_y), and shear (F_x or F_y) stiffnesses that account for the contribution of all the wall panels can be computed as:

$$A_z = \sum_{i=1}^{n} \bar{A}_i b_i$$

$$B_y = \sum_{i=1}^{n} [\bar{A}_i(\bar{y}_i - y_n) + \bar{B}_i \cos\phi_i] b_i$$

$$D_y = \sum_{i=1}^{n} \left[\bar{A}_i \left((\bar{y}_i - y_n)^2 + \frac{b_i^2}{12} \sin^2\phi_i \right) \right. \qquad (7)$$

$$\left. + 2\bar{B}_i(\bar{y}_i - y_n)\cos\phi_i + \bar{D}_i \cos^2\phi_i \right] b_i$$

$$F_y = \sum_{i=1}^{n} \bar{F}_i b_i \sin^2\phi_i$$

The location of the neutral axis of bending (x_n or y_n), as shown in Figure 3, can be defined by equating to zero the beam bending-extension coupling coefficient (B_x or B_y). An explicit expression for the static shear correction factor (K_x or K_y) is derived from energy equivalence, and the location of the shear center is defined in order to avoid geometric coupling of bending and torsion. General equations for the static shear correction factor for various FRP sections are presented in Reference [13]. Displacement and rotation functions can be obtained by solving Timoshenko's beam theory equilibrium equations. In particular, available expressions for maximum bending and shear deflections can be used; for example, the maximum deflection for a 3-point loading of a beam of span L and design load P is:

$$\Delta = \Delta_b + \Delta_s = \frac{PL^3}{48D_y} + \frac{PL}{4K_yF_y} \qquad (8)$$

As illustrated in Equation (8), the bending and shear components of deflection can be independently evaluated in MLB.

3.2 Predictions of Ply Strains and Stresses and First-Ply-Failure

For a beam loaded in the z–y plane (Figure 3), the axial, shear, and bending stress resultants are N_z, V_y, and M_y. Then, the middle-surface strains and curvature of the ith wall are expressed as

$$\bar{\varepsilon}_z(s_i, z) = \frac{N_z}{A_z} + (y(s_i) - y_n)\frac{M_y}{D_y}, \quad \bar{\gamma}_{sz}(s_i, z) = \frac{V_y}{K_yF_y}\sin\phi_i$$
$$\bar{\chi}_z(s_i, z) = \frac{M_y}{D_y}\cos\phi_i \qquad (9)$$

and the stress resultants in the ith wall become

$$\bar{N}_z(s_i, z) = \bar{A}_i\bar{\varepsilon}_z + \bar{B}_i\bar{\chi}_z, \quad \bar{N}_{sz}(s_i, z) = \bar{F}_i\bar{\gamma}_{sz}$$
$$\bar{M}_z(s_i, z) = \bar{B}_i\bar{\varepsilon}_z + \bar{D}_i\bar{\chi}_z \qquad (10)$$

Ply strains and stresses, through the thickness of the ith wall, can be obtained from Classical Lamination Theory (CLT) [14] using the stress resultants given in Equations (10). The accuracy of MLB for deflections and strains has been favorably established experimentally and numerically (see Reference [8]).

The Tsai-Hill failure criterion is used to predict the first-ply-failure (FPF) factor for a given load as

$$\text{FPF} = K_{SF}\sqrt{\left[\left(\frac{\sigma_1}{X}\right)^2 + \left(\frac{\sigma_2}{Y}\right)^2 - \frac{\sigma_1\sigma_2}{X^2} + \left(\frac{\tau_{12}}{S}\right)^2\right]} \qquad (11)$$

where K_{SF} is a safety factor greater than one; as an illustration in this study, a value of 3.0 is used, to account for uncertainties in modeling, particularly ply strength values. The in-plane stress components σ_1, σ_2, and τ_{12} are defined in material coordinates, and X, Y, and S are the corresponding ply strengths, as given, for example,

...l Table 1. A value of FPF lower than 1.0 indicates that first-ply-failure is not of concern in the design.

3.3 FRPBEAM Computer Program

Based on the modeling assumptions and analytical tools for FRP beams discussed previously, the computer program FRPBEAM was developed by Qiao, Davalos and Barbero [15] to model, analyze and design FRP beams, from the evaluation of ply stiffnesses by micromechanics [9] to the overall beam response by Mechanics of Laminated Beams (MLB) [13]. As previously verified by a combined experimental and numerical study [8,16], the MLB subroutine can be used to confidently predict displacements and strains for pultruded FRP beams.

3.4 Elastic Buckling of FRP Shapes

To predict the critical buckling loads and buckling modes, we use in this study 8-node isoparametric layered shell finite elements with ANSYS [17]. Due to the relatively low stiffness-to-strength ratio of glass fiber-reinforced pultruded sections, the cross sections, consisting of thin or moderately thick walls or panels, usually have large depths, and both local-distorsional and lateral-torsional buckling effects should be considered in design. For compact or closed cross sections, lateral-torsional buckling may not be critical, but local buckling can be important particularly for thin-walled sections. We indicate the buckling response using a buckling load factor (BLF), which is a ratio of the design load, P, to the critical buckling load, P_{cr}:

$$\text{BLF} = K_{SF}\,\frac{P}{P_{cr}} \tag{12}$$

where K_{SF} is a safety factor; as an illustration, a value of $K_{SF} = 3.0$ is used in this study. A value of BLF smaller than 1.0 indicates that buckling is of no concern. In this study, the critical buckling load obtained from ANSYS is used in analysis and optimization, and no effort is made to correlate the critical buckling load to the corresponding buckling mode.

4. DESIGN PROBLEM FORMULATION AND OPTIMIZATION SCHEME

In this section, we describe the formulation of the design optimization problem and the proposed optimization scheme. The optimal design of pultruded FRP structural shapes is a standard problem of finding a design variable vector $\mathbf{b}$ that will minimize an objective function $F(\mathbf{b})$ subjected to equality constraints, $G_i(\mathbf{b}) = 0$ ($i = 1$ to p), and inequality constraints, $G_i(\mathbf{b}) \le 0$ [$i = (p+1)$ to m], and with explicit lower and upper bounds on the design variables given as $b_{il} \le b_i \le b_{iu}$, for $i = 1$ to n.

In this study, the objective function represents the cross-sectional area of FRP shapes, and the minimization of the beam cross-sectional area can be accomplished with available unconstrained optimization algorithms. However, the evaluation of the constraints (deflections, structural failure, critical buckling loads) can be a difficult problem and a time-consuming effort involving explicit and/or numerical analyses to define the design space. For a given shape, we define the geometric constraints based on practical applications [8], and the constituent materials and lay-up system are defined based on material availability and manufacturing limitations, as presented in Section 2.

The optimization scheme, OPTSHAPE, used in this study is illustrated in Figure 4. The constraints on deflection limit, first-ply-failure load, and critical buckling load are generated through global approximations using the FRPBEAM program [15] and finite element analysis with ANSYS [17]. Then, the beam midspan deflection (Δ), first-ply-failure (FPF) factor, and buckling load factor (BLF) are evaluated at a number of design points (dimensional and material-architecture variables) and expressed in terms of the design variables through multiple linear regression analysis (MLRANA) to generate power law expressions. In OPTSHAPE, the constraint functions are defined through a global approximation [2], and they are subsequently refined in an iterative process as the optimization evolves. The most common global approximation used is the response surface approach. With this approach, the constraint function is sampled at a number of design points (a set of dimensional and material variables), and then an analytical expression called the response surface (a polynomial) is fitted to the data. Construction of a response surface often relies heavily on the theory of experi-

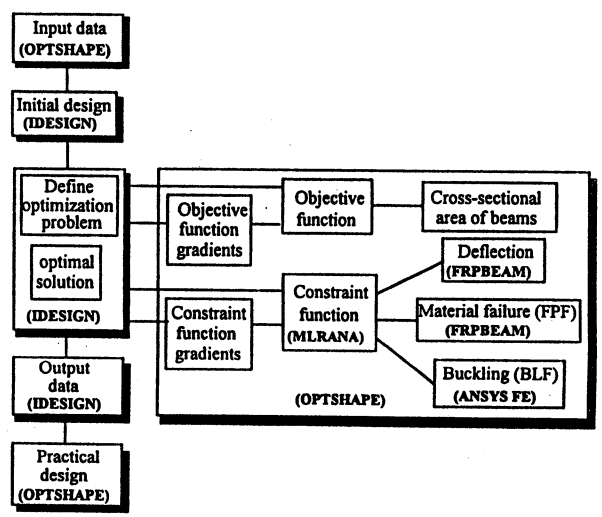

Figure 4. *Optimization scheme of OPTSHAPE.*

ments and is an iterative process that begins with the assumption of the analytical form of the response surface. In this study, we use a multiple linear regression analysis (MLRANA) to generate the response surface. Then, the approximate model (the response surface) is used to predict the function at a number of selected test points (a selected set of design variables), and statistical measures are used to assess the goodness-of-fit, or the accuracy, of the response surface. If the fit is not satisfactory, the process is restarted, and further experiments are made, or the postulated model is improved by removing and/or adding terms. Finally, the approximation model generates a power law as a constraint function of design variables.

Several design variables should be considered in the optimization of composite shapes. The geometric cross-sectional variables include the thickness and width, or height, of each panel. The material variables include the lamination sequence, a variety of resin and fiber systems, fiber orientations, and fiber volume fractions (V_f). Manufacturing constraints in the pultrusion process should be considered to eliminate or limit some of these variables, such as lamination sequence and fiber volume fractions. Based on the characterization of ply materials introduced in Section 2, we assume a $(3m - 1)$ symmetric lay-up system for a given panel of a

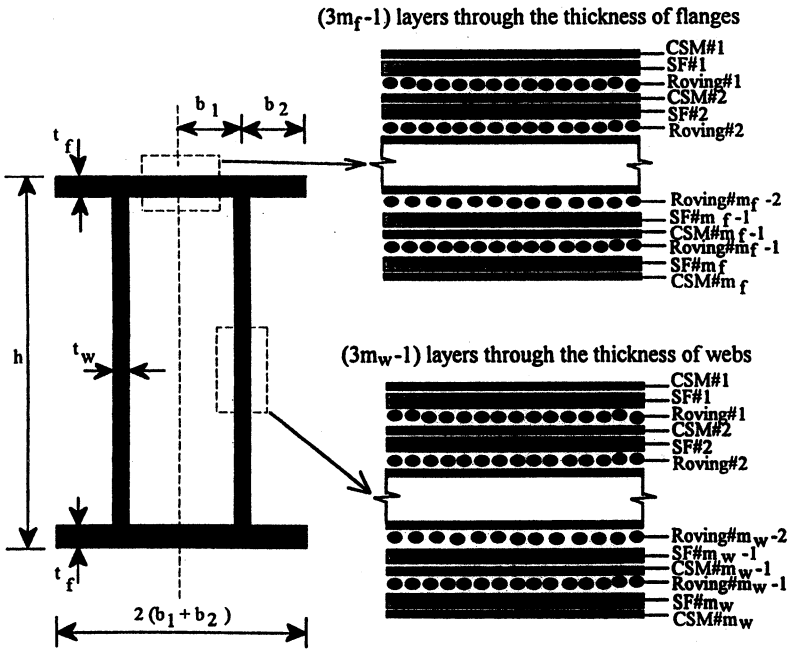

Figure 5. Cross-sectional dimensions and material architecture of winged-box (WB) section.

pultruded FRP beam, and the lay-up number m and roving layer thickness t_r are considered as the panel material-architecture design variables. The panel thicknesses and the corresponding fiber percentages of roving, CSM and ±45° angle-ply stitched fabrics can be determined from these two design variables (see Section 2). Considering material-architecture variables and dimensional variables, we proceed to optimize an FRP shape.

In Figure 4, OPTSHAPE consists of several subroutines that perform the analyses of new pultruded FRP shapes and define the optimization problem to be solved with IDESIGN [6], which is used as an optimization program. For specified input data, the objective and constraint functions are generated by the program OPTSHAPE. At each iteration in the design process, updated values of the deflections, first-ply-failure factors (FPF), and buckling load factors (BLF) are computed by the structural analysis subroutines of OPTSHAPE to generate the constraint functions.

As an application, a new winged-box (WB) pultruded FRP shape (Figure 5) is optimized using the optimization scheme of Figure 4. The details of the optimization of the winged-box beams are presented in the next section, and a similar procedure can be applied to optimize other innovative FRP shapes.

5. OPTIMIZATION OF FRP WINGED-BOX (WB) BEAMS

A pultruded FRP Winged-Box (WB) section as a new structural shape has promising advantages for future applications in civil structures. The main features of a WB section are: 1) the closed-section geometry provides a higher torsional stiffness than conventional open-sections; hence, the response of this section to torsional warping and lateral-torsional buckling can be highly improved; 2) the double-web configuration of the WB section provides about twice the shear stiffness of a conventional wide-flange (WF) shape; 3) the WB section can provide better bending stiffness about the weak axis than a box section; 4) the shear-lag and local buckling effects in the flanges of a WB section are reduced because of the presence of the two stiffening webs. Also, the two webs provide a better stress distribution between webs and flanges than in a WF section; 5) finally, the wing flanges can facilitate the connection details to other members, such as columns and decks or wall panels.

5.1 Optimal Design Problem Formulation for FRP Winged-Box (WB) Beams

The selected load and span combination is intended for application in short-span bridges under AASHTO HS 25-44 traffic loading. The optimal design problem is concerned with simply-supported beams under a midspan concentrated load. The equivalent maximum transverse load is $P_y = 53{,}400$ N [12,000 lb], and the beam span is $L = 6.096$ m [20.0 ft]. The optimal design of the winged-box section is a minimization problem of the cross-sectional area with design variables subjected to inequality constraints. The objective function for the winged-box section is the cross-sectional area (as shown in Figure 5), defined as:

$$A = 2[2(b_1 + b_2)t_f + ht_w] \tag{13}$$

where as shown in Equation (1), the thicknesses of flanges (t_f) and webs (t_w) can be expressed as

$$\begin{aligned} t_f &= m_f t_{SF} + m_f t_{CSM} + (m_f - 1)t_{rf} \\ t_w &= m_w t_{SF} + m_w t_{CSM} + (m_w - 1)t_{rw} \end{aligned} \tag{14}$$

The subscripts f and w relate quantities to flange and web panels, respectively; m is the lay-up number, with $(3m_f - 1)$ and $(3m_w - 1)$ as the total number of layers on flange and web panels, and t_{rf} and t_{rw} are, respectively, the roving layer thicknesses on the flange and web panels. The seven design variables of the optimization problem are: b_1, b_2, h, m_f, t_{rf}, m_w and t_{rw}. The material architectures for the flanges and webs of the WB section are both symmetric but can be different from each other, because of differences in the lay-up numbers and roving layer thicknesses (Figure 5). The material configurations consist of rovings (unidirectional fibers), continuous strand mats (CSM), and ±45° angle-ply stitched fabrics (SF) arranged in a symmetric pattern (see details in Section 2). The optimal thicknesses of flanges and webs can be obtained from the optimized material architectures (by knowing m_f, t_{rf}, m_w, and t_{rw} in the optimization process).

A multiple linear regression analysis (MLRANA) is used to generate the approximate constraint functions in terms of natural logarithms:

$$\begin{aligned} \ln(F) = {} & \alpha + \beta \ln(b_1) + \chi \ln(b_2) + \delta \ln(h) + \varepsilon \ln(m_f) \\ & + \phi \ln(t_{rf}) + \gamma \ln(m_w) + \eta \ln(t_{rw}) \end{aligned} \tag{15}$$

where, F represents the function defining either midspan deflection (Δ), or BLF, or FPF, and $\alpha, \beta, \chi, \delta, \varepsilon, \phi, \gamma$ and η are unknown constants. Then, the approximate function of Equation (15) is used to generate a power law as a constraint function of design variables:

$$F(\Delta, \text{ or FPF or BLF}) = \alpha b_1^{\beta} b_2^{\chi} h^{\delta} m_f^{\varepsilon} t_{rf}^{\phi} m_w^{\gamma} t_{rw}^{\eta} \tag{16}$$

Based on practical considerations, the lower and upper bounds on the design variables are:

$$76.2 \text{ mm } [3.0 \text{ in}] \le b_1 \le 228.6 \text{ mm } [9.0 \text{ in}]$$

$$50.8 \text{ mm } [2.0 \text{ in}] \le b_2 \le 152.4 \text{ mm } [6.0 \text{ in}]$$

$$304.8 \text{ mm } [12.0 \text{ in}] \le h \le 609.6 \text{ mm } [24.0 \text{ in}]$$

$$2 \le m_f \le 9$$

$$0.0508 \text{ mm } [0.002 \text{ in}] \le t_{rf} \le 17.018 \text{ mm } [0.67 \text{ in}] \text{ (see Figure 2)}$$

$$2 \le m_w \le 9$$

$$0.0508 \text{ mm } [0.002 \text{ in}] \le t_{rw} \le 17.018 \text{ mm } [0.67 \text{ in}] \text{ (see Figure 2)} \tag{17}$$

Using these limits, the evaluations of deflections (Δ), first ply failure factors (FPF), and buckling load factors (BLF) are carried out using the analytical tools introduced in Section 3, for a finite set of design variables. The results of the parametric studies are used to generate power functions [Equation (16)] for the constraints Δ, FPF, and BLF.

Four design constraints are considered.

1. Flange and web panel thicknesses:

$$t_f = m_f t_{SF} + m_f t_{CSM} + (m_f - 1)t_{rf} \le 19.05 \text{ mm } [0.75 \text{ in}] \tag{18}$$

$$t_w = m_w t_{SF} + m_w t_{CSM} + (m_w - 1)t_{rw} \le 19.05 \text{ mm } [0.75 \text{ in}] \tag{19}$$

   where, 19.05 mm [0.75 in] is the approximate maximum thickness that can be produced by existing pultrusion technology.
2. Deflection limit (FRPBEAM program):

$$\begin{aligned} \Delta = {} & 0.0660 \text{ mm } [910.8262 \text{ in}]\, b_1^{-0.39047} b_2^{-0.25333} h^{-2.22212} \\ & \times m_f^{-1.17995} t_{rf}^{-0.66389} m_w^{-0.81055} t_{rw}^{-0.41692} \le \frac{L}{800} \end{aligned} \tag{20}$$

   where, L is the length of the beam (= 6.096 m [20.0 ft] in this study), an $L/800$ is a limit commonly used in bridge design.
3. Material failure (first-ply-failure by Tsai-Hill Failure criterion, FRPBEAM program):

$$\begin{aligned} \text{FPF} = {} & 52.9353 b_1^{-0.332328} b_2^{-0.296957} h^{-1.330647} m_f^{-0.946984} \\ & \times t_{rf}^{-0.597288} m_w^{-0.862306} t_{rw}^{-0.466959} \le 1.0 \end{aligned} \tag{21}$$

4. Finally, elastic buckling analysis (buckling load factor with ANSYS, FE):

$$\begin{aligned} \text{BLF} = {} & 1.17415 b_1^{-0.751492} b_2^{0.02388} h^{0.0626} m_f^{-0.77724} \\ & \times t_{rf}^{-0.434566} m_w^{-1.393682} t_{rw}^{-0.751492} \le 1.0 \end{aligned} \tag{22}$$

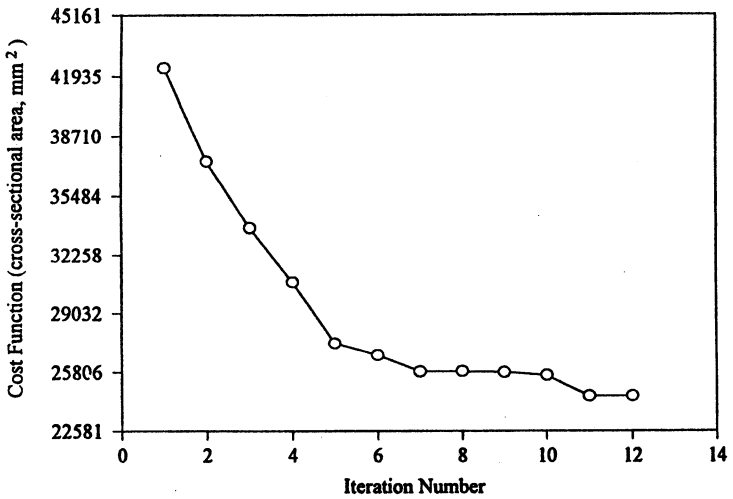

Figure 6. *Cost function (cross-sectional area) history.*

By combining the OPTSHAPE and IDESIGN programs (Figure 4), the optimized solution for the winged-box section is obtained through several iterations (Figure 6). The optimum design for the cross-sectional geometry and material architecture for the winged box (WB) section is given in Table 2, and the constraint values at the optimum design point are shown in Table 3.

To examine the goodness-of-fit of the multiple linear regressions [Equation (15)] for the constraint functions [Equations (20) to (22)], the confidence intervals

Table 2. Evolution of design variables for winged box (WB) beam for selected iterations.

	No. of Iterations			
	7	9	10	12 (opt.)
b_1 (mm)	102.46	79.17	76.20	**76.20**
b_2 (mm)	79.48	102.49	93.88	**80.75**
h (mm)	389.99	459.21	547.80	**609.60**
m_f	3.578	4.601	5.354	**5.846**
t_{rf} (mm)	8.128	5.283	3.683	**2.819**
m_w	6.865	8.775	9.000	**9.000**
t_{rw} (mm)	0.114	0.119	0.117	**0.109**
A (mm^2)	26174.1	26247.0	25633.5	**24510.9**
Max. Vio.*	1.658	0.0660	0.0222	**0.0187**
Conv. Parm.**	1.000	3.151	0.0707	**0.0654**

*Maximum constraint violation (Max. Vio.) should be nearly zero for feasible design.
**Convergence Parameter (Conv. Parm.) should be nearly zero for optimum design cost.

Table 3. Deflection (Δ), FPF and BLF factors at the optimum point.

Constraint Function	Values at Optimum Point
Deflection (Δ)	7.772 mm
Material failure (FPF factor)	0.509
Buckling (BLF)	0.842

Table 4. Predictions at the optimum design point with 90% confidence.

			90% Confidence Intervals	
Constraint Function	Predicted Optimum Value	Measure of Standard Deviation	Lower Limit	Upper Limit
Δ	7.772 mm	1.072 mm	6.008 mm	9.535 mm
FPF	0.509	0.0689	0.396	0.622
BLF	0.842	0.0868	0.699	0.985

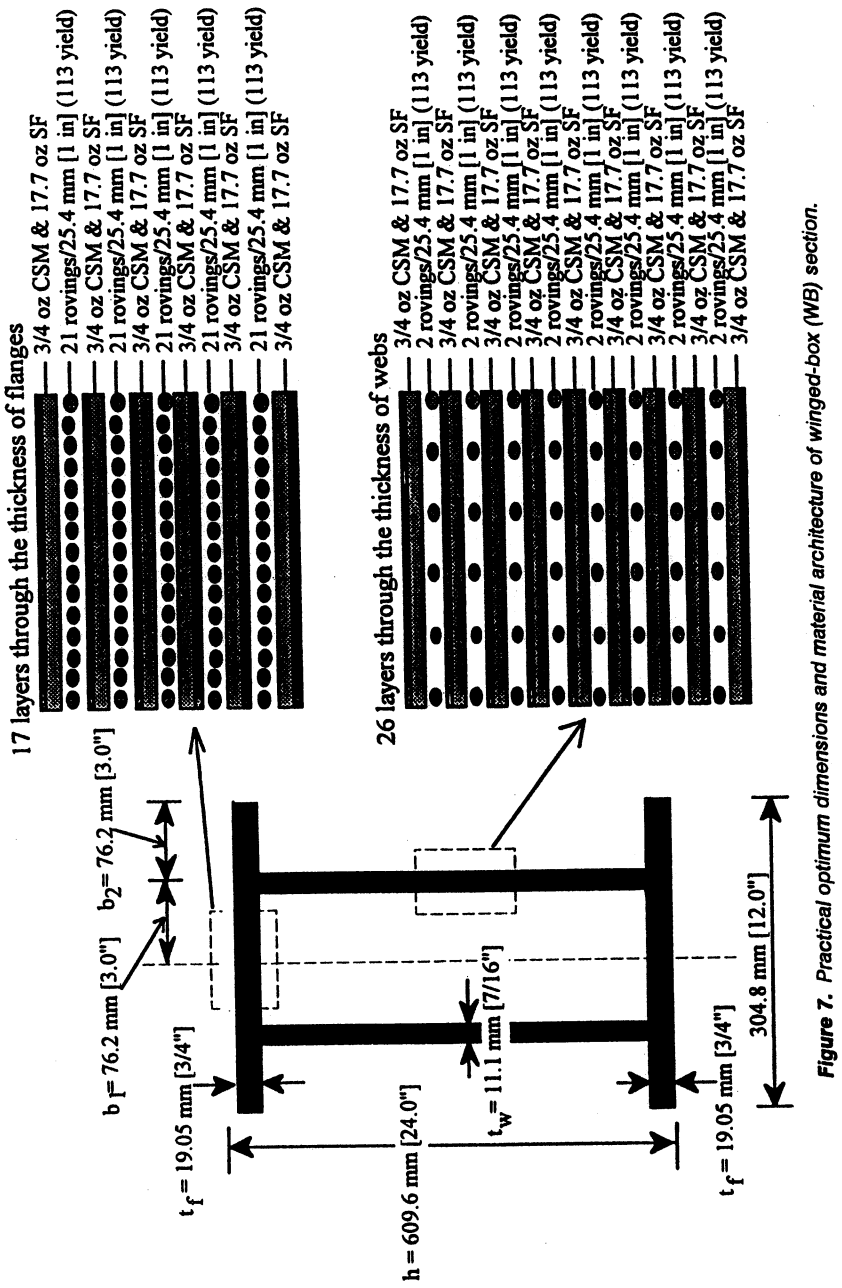

Figure 7. Practical optimum dimensions and material architecture of winged-box (WB) section.

Table 5. Fiber percentages of typical layers for the optimum winged-box (WB) section.

Layers	Fiber Percentages (%)		
	In Flanges	In Webs	In the Whole Section
3/4 oz. CSM (X_{CSM})	2.832	7.282	4.471
17.7 oz. ±45° SF (X_{SF})	7.140	18.360	11.274
113 yield rovings (X_r)	37.400	9.735	27.208
Total	47.372	35.377	42.953

are estimated [18]. In Table 4, we show the predicted values for Δ, FPF, and BLF along with approximations of standard deviations (usually denoted as *s*); the limits around the mean (optimum) values for 90% confidence intervals indicate relatively narrow distributions (about 20%) above and below the predicted optimum values.

As can be observed from the optimization results (Table 3), both the deflection and elastic buckling constraints are the primary influential factors in the design of the WB FRP beam, with material failure being less of a concern for the type of load selected in this example.

5.2 Results of Winged-Box (WB) Beam Optimization

Based on the results presented in the previous section, the final practical dimensions and detailed material architecture of the winged-box (WB) beam are shown in Figure 7. The materials chosen are commercially available and currently used by the pultrusion industry. The fiber percentages of CSM, angle-ply SF, and roving layers in the optimum WB section are different for flanges and webs, and the results are listed in Table 5 [computed from Equation (3)]. A reanalysis of this section indicates the following results: deflection Δ = 7.645 mm [0.301 in](≈ *L*/800); material failure factor (FPF) = 0.393, which takes place in the ±45° angle-ply fabric layer of the webs at the junction with the flanges; and buckling load factor, BLF = 0.534, corresponding to local buckling mode of the beam panels. The lay-up shown in Figure 7 can be used in industry to manufacture this potential section, and therefore, the optimization procedure presented in this paper is a practical tool to develop new FRP shapes.

6. CONCLUSIONS

The results presented in this paper indicate that practical optimal solutions for FRP shapes can be obtained by using the existing knowledge on FRP shapes and an innovative optimization technique, as described in this study. The global approximation approach is successful in handling the constraint functions, which are the most difficult to define in a design optimization process. In this study, the multiple linear regression constraint equations provide smooth fitting-functions in the

multi-dimensional design space and are used to define power-law approximations of the constraints as products of the design variables. The analytical tools used to characterize the structural behavior of FRP shapes provide a vehicle to carry out the optimization process. It is significant that through this work, a new optimal shape of a winged-box section is proposed for structural applications, and the present technique can be used to develop various new shapes. Thus, the present approach can permit the development of a new family of efficient FRP geometries for the civil structural market.

REFERENCES

1. Abrate, S. 1994. "Optimal Design of Laminated Plates and Shells," *Composite Structures,* 29:269–286.
2. Haftka, R. T. and Z. Gurdal. 1992. *Elements of Structural Optimization,* Boston, MA: Kluwer Academic Publishers.
3. Burnside, P., E. J. Barbero and J. F. Davalos. 1993. "Design of an All-FRP Short-Span Bridge," *Proc. of 11th Structural Congress,* ASCE, Irvine, CA, 2:1390–1395.
4. Morton, S. K. and J. P. H. Webber. 1994. "Optimal Design of a Composite I-Beam," *Composite Structures,* 28:149–168.
5. Davalos, J. F., P. Qiao and E. J. Barbero. 1996. "Multiobjective Material Architecture Optimization of Pultruded FRP I-Beams," *Composite Structures,* 35:271–281.
6. Arora, J. S. 1989. *IDESIGN User's Manual,* Optimal Design Laboratory, The University of Iowa, Technical Report No. ODL-89.7, Iowa City, Iowa.
7. Barebero, E. J. 1991. "Pultruded Structural Shapes—From the Constituents to the Structural Behavior," *SAMPE Journal,* 27:25–30.
8. Davalos, J. F., H. A. Salim, P. Qiao, R. Lopez-Anido and E. J. Barbero. 1996. "Analysis and Design of Pultruded FRP Shapes under Bending," *Composites: Part B, Engineering Journal,* 27B:295–305.
9. Luciano, R. and E. J. Barbero. 1994. "Formulas for the Stiffness of Composites with Periodic Microstructure," *Int. J. of Solids and Structures,* 31:2933–2944.
10. Makkapati, S. 1994. "Compressive Strength of Pultruded Structural Shapes," M.S. Thesis, West Virginia University, Morgantown, WV.
11. Sonti, S. S. 1992. "Stress Analysis of Pultruded Structural Shapes," M.S. Thesis, West Virginia University, Morgantown, WV.
12. Tomblin, J. S. 1994. "Compressive Strength Models for Pultruded Glass Fiber Reinforced Composites," Ph.D Dissertation, West Virginia University, Morgantown, WV.
13. Barbero, E. J., R. Lopez-Anido and J. F. Davalos. 1993. "On the Mechanics of Thin-Walled Laminated Composite Beams," *J. Composite Materials,* 27:806–829.
14. Jones, R. M. 1975. *Mechanics of Composite Materials,* New York, NY: Hemisphere Publishing Corporation.
15. Qiao, P., J. F. Davalos and E. J. Barbero. 1994. "FRPBEAM: A Computer Program for Analysis and Design of FRP Beams," *CFC-94-191,* Constructed Facilities Center, West Virginia University, Morgantown, WV.
16. Davalos, J. F. and P. Qiao. 1996. "A Computational Approach for Analysis and Optimal Design of FRP Beams," submitted ot *Computers and Structures.*
17. DeSalvo, G. J. and R. W. Gorman. 1989. *ANSYS User's Manual,* Revision 4.4, Swanson Analysis System, Inc., Houston, PA.
18. Neter, J., M. H. Kutner, C. J. Nachtsheim and W. Wasserman. 1990. *Applied Linear Regression Models,* Chicago, IL.: Irwin.

EDITORIAL POLICY

"The primary purpose of the *Journal of Composite Materials* is to provide a permanent record of achievements in the science, technology, and economics of composite materials. Implicit in this objective is the recognition and appropriate publication of the accomplishments of all participating interests.

"Fulfillment of this purpose depends almost entirely upon the voluntary contribution of articulate, accurate, and authoritative manuscripts. In addition to the multiple reviewing of candidate manuscripts to assure high standards of technical veracity, editorial selectivity also involves consideration of the equitable coverage of the entire field.

"In further discharging its responsibilities, the journal endorses the content and programs of appropriate trade associations and professional societies, but asserts its independent role in both the recording and, if necessary, appraising of their activities."

INSTRUCTIONS FOR AUTHORS

Submitting Papers to the Journal:

1. Three copies should be submitted to Editor, H. Thomas Hahn, Journal of Composite Materials, Hughes Aircraft Co. Professor, University of California, Los Angeles, MANE Department, Eng. IV, Los Angeles, CA 90024-1597.
2. Title should be brief, followed by name, affiliation, address, country, and postal code (zip) of author(s). Indicate to whom correspondence and proofs should be sent, including a telephone number.
3. Include a 100-word abstract, key words, and author(s) biographies.
4. Submit three copies also of camera-ready drawings and glossy photographs. Drawings should be uniformly sized, if possible, planned for 50% reduction. Both line drawings and photographs must be called out in the text. Appropriate captions should all be typed on one sheet.
5. Journal and book references should be identified in the text by enclosing in brackets and should be numbered in order. Literature references should be listed at end of manuscript, using following style:

   Journal: Halpin, J. C. 1967. J. Cellular Plastics, 3:432-435.
   Book: Ouellette, R. P. and P. N. Cheremisinoff. 1985. Applications of Biotechnology. Lancaster, PA: Technomic Publishing Co., Inc.

6. Tables. Number consecutively and type on a numbered, separate page. Please use arabic numerals and supply a heading. Column headings should be explanatory and carry units (see example at right).

Table 5. Comparison of state-of-the-art matrix resins with VPSP/BMI copolymers.

Resin System	Core Temp. (DSC peak), °C	T_E, °C	PDT(N_2) °C	Char Yield, %
Epoxy (MY720)	235	250	300	30
Bismaleimide (H795)	282	>400	400	48
VPSP/Bismaleimide copolymer				
C379: H795 = 1.9	245	>400	400	50
C379: H795 = 1.4	285	>400	400	53

7. Units & Abbreviations. SI units should be used. English units or other equivalents should appear in parentheses if necessary.
8. Symbols. A list of symbols used and their meanings should be included if a large number of symbols appears in the text.
9. Proofreading and Reprints. Authors will receive galley or page proofs, which they should correct and return as soon as possible. Also submit key words of your contribution on separate sheet provided. This is important in helping us to construct the index. Authors will also receive a reprint order form.
10. Copyright Information. All journal articles are copyrighted in the name of the publisher, except in the event of prior copyright by an author.
11. Headings. Your article should be structured with headings. Normally two headings are used as follows:

    Main Subhead: DESIGN OF A MICROWAVE INSTALLATION
    Secondary Subhead: Principle of the Design Method

    If further subordination is required, please limit to no more than one, or two at the most.
12. Equations. Number equations with arabic numbers enclosed in parentheses at the right-hand margin. Type superscripts and subscripts clearly above or below the baseline, or mark them with a caret: T^{2}_{a}. Be sure that all symbols, letters, and numbers are distinguishable (e.g., "oh" or zero, one or lowercase "el," "vee" or Greek nu). Handwritten Greek letters should be identified by spelling them out in the margin.
13. Permissions. The author is responsible for obtaining releases from other publishers for Technomic Publishing Company, Inc. to publish material copyrighted by someone else.

GENERAL

The *Journal of Composite Materials* is not responsible for the views expressed by individual contributors in articles published in the Journal.